Efficient simulation of unitary operators by combining two numerical algorithms: An NMR simulation of the mirror-inversion propagator of an XY spin chain

K. Rama Koteswara Rao,[1] T. S. Mahesh,[2] and Anil Kumar[1]

[1]*Centre for Quantum Information and Quantum Computation, Department of Physics and NMR Research Centre, Indian Institute of Science, Bangalore 560012, India*

[2]*Department of Physics and NMR Research Center, Indian Institute of Science Education and Research, Pune 411008, India*

(Received 24 July 2013; revised manuscript received 27 February 2014; published 8 July 2014)

Precise experimental implementation of unitary operators is one of the most important tasks for quantum information processing. Numerical optimization techniques are widely used to find optimized control fields to realize a desired unitary operator. However, finding high-fidelity control pulses to realize an arbitrary unitary operator in larger spin systems is still a difficult task. In this work, we demonstrate that a combination of the GRAPE algorithm, which is a numerical pulse optimization technique, and a unitary operator decomposition algorithm [Ajoy *et al.*, Phys. Rev. A **85**, 030303 (2012)] can realize unitary operators with high experimental fidelity. This is illustrated by simulating the mirror-inversion propagator of an XY spin chain in a five-spin dipolar coupled nuclear spin system. Further, this simulation has been used to demonstrate the transfer of entangled states from one end of the spin chain to the other end.

DOI: 10.1103/PhysRevA.90.012306 PACS number(s): 03.67.Lx, 03.67.Ac, 82.56.−b

I. INTRODUCTION

Designing control pulses to precisely implement unitary operators, i.e., effective Hamiltonians, is one of the most important tasks for quantum information processing. Numerical optimization techniques have been proposed and are being commonly used for such a purpose [1,2]. However, due to their extensive numerical complexity, finding robust and high-fidelity control pulses to realize an arbitrary unitary operator even in a five-spin system would be a difficult task. Consider the GRAPE algorithm [2], an efficient and one of the most widely used algorithms, which is based on the numerical optimal control approach. *A priori* knowledge about the approximate time duration of the pulses will be very helpful for this algorithm to find high-fidelity pulse sequences to accurately implement a desired unitary operator. However, in the case of an arbitrary unitary operator, this information is not known beforehand, and a lot of time is usually spent in finding the optimal time duration using trial and error methods.

There are also many numerical algorithms to decompose an arbitrary unitary operator into a circuit consisting of single- and two-qubit gates [3–6]. The algorithm proposed by Ajoy *et al.* [6] exploits the symmetry of the unitary operator and, in favorable cases, it can give polynomial product decompositions. One of the advantages of this algorithm is that it can provide decompositions into a chosen operator basis. For example, decompositions into the Pauli operator basis (gates such as ZZ) would be easier to implement compared to the CNOT gates in spin-based quantum architectures such as nuclear magnetic resonance (NMR).

Here, we demonstrate that a combination of the GRAPE algorithm and Ajoy's algorithm can be useful for precise experimental implementations of unitary operators. For this purpose, we chose to simulate the mirror-inversion propagator corresponding to the time evolution of an engineered XY spin chain [7]. In the last decade, there have been many interesting proposals in using spin chains to efficiently transfer quantum information between different parts of a quantum information processor [8–22]. Some of these proposals have also been experimentally verified [23–29]. Albanese *et al.* [7] have shown that mirror inversion of quantum states with respect to the center of an XY spin chain can be achieved by modulating its coupling strengths along the length of the chain. The advantage of this protocol is that nontrivial entangled states of multiple qubits can be transferred from one end of the chain to the other end.

In this work, we first product decompose the mirror-inversion propagators of four- and five-spin XY chains into the Pauli operator basis using Ajoy's algorithm. These decompositions, which only scale linearly with the number of spins, have also been extended to N-spin chains. Then, the control pulses to realize each of the decomposed four-spin and five-spin unitary operators are found using the GRAPE algorithm. There are several advantages to this approach. First of all, it is always easy to optimize control pulses for smaller unitary operators. Second, the approximate time duration of the pulses to realize the decomposed unitary operators can be estimated beforehand, which saves a lot of time during optimization. The decomposed operators can be further decomposed into rotations about x and y axes and two-spin operators [30]. Hence, by optimizing control pulses only for a universal set of single- and two-qubit operators, one can implement any desired unitary operator. The subsystems approach used in Refs. [31,32] can also be combined with this method to realize unitary operators in larger spin systems. The high experimental fidelities achieved in this work indicate the efficiency of the above method.

The experiments have been performed in a five-qubit nuclear spin system, partially oriented in a liquid-crystal medium, using NMR techniques. The spins are thus coupled by residual dipolar couplings as well as indirect scalar couplings [33]. The residual dipolar couplings are an order of magnitude stronger than the scalar couplings, which are frequently used to realize multiqubit gates in liquid-state NMR quantum information processing [34,35].

The paper is arranged as follows. In Sec. II, we describe the mirror-inversion operation in an engineered XY spin chain and

 ©2014 American Physical Society

the product decomposition of the corresponding propagator into the Pauli operator basis. In Sec. III, we present the experimental implementation. In Sec. IV, we compare this simulation with the mirror-inversion operation by a set of SWAP gates, and in Sec. V we conclude.

II. MIRROR-INVERSION PROPAGATOR AND SIMULATION

Consider a chain of N spin-1/2 particles, coupled by nearest-neighbor XY interaction, with the Hamiltonian

$$\mathcal{H} = \frac{1}{2}\sum_{i=1}^{N-1} J_i\left(\sigma_i^x\sigma_{i+1}^x + \sigma_i^y\sigma_{i+1}^y\right) + \frac{1}{2}\sum_{i=1}^{N} h_i\left(\sigma_i^z + 1\right). \quad (1)$$

Here, $\sigma_i^{x/y/z}$ are the Pauli matrices for the spin i, J_i is the coupling between the spins i and $i+1$, and h_i is the local magnetic field at the spin site i. In Refs. [7,15], it was theoretically shown that mirror-inversion operation with respect to the center of this chain can be achieved using only the natural unitary evolution of the spin chain by engineering its interactions (J_i, h_i). To be precise, let us consider the state $\Psi(s_1,s_2,\ldots,s_N)$, where $s_n = 0,1$, as the initial state of the spin chain. Then, for some time τ,

$$\exp(-i\mathcal{H}\tau)\Psi(s_1,s_2,\ldots,s_N) = \Psi(s_N,s_{N-1},\ldots,s_1). \quad (2)$$

Apart from transferring the quantum state of a qubit to its mirror site, the mirror-inversion operation in spin chains can also be used to transfer entangled states of multiple qubits to their mirror sites.

Here, we consider the above XY spin chain with the interactions $J_i = \sqrt{i(N-i)}, h_i = 0$. It was shown [7] that this spin chain achieves mirror inversion for a time $\tau = \pi/2$. In the following, we first describe the product decompositions of the mirror-inversion propagators $[U_{XY}(\frac{\pi}{2}) = \exp(-i\mathcal{H}\frac{\pi}{2})]$ of the four- and five-spin XY spin chains into the Pauli operator basis using Ajoy's algorithm. Then we extend the decomposition to N-spin XY chains.

A. Four-spin chain

The values of the nearest-neighbor coupling constants for the four-spin XY chain are $J_1 = \sqrt{3}$, $J_2 = 2$, $J_3 = \sqrt{3}$. For simplicity, we refer to $U_{XY}(\frac{\pi}{2})$ as U_{XY}.

The Pauli operator basis for the four-spin system is given by

$$B = \left\{\sigma_1^\alpha\sigma_2^\beta\sigma_3^\gamma\sigma_4^\delta\right\}, \quad (3)$$

where $\alpha,\beta,\gamma,\delta \in \{0,x,y,z\}$ and $\sigma^0 = \mathbb{1}$. Our aim is to product decompose U_{XY} into the Pauli operator basis as follows:

$$U_{XY} = \prod_{k=1}^{m}\exp(-i\theta_k D_k); \quad D_k \in B. \quad (4)$$

Since B forms a complete basis, U_{XY} can be expanded as a sum in B as follows:

$$U_{XY} = \frac{1}{4}\sum_{\alpha,\beta}\eta_{\alpha\beta}\left(\sigma_1^\alpha\sigma_2^\beta\sigma_3^\beta\sigma_4^\alpha\right), \quad (5)$$

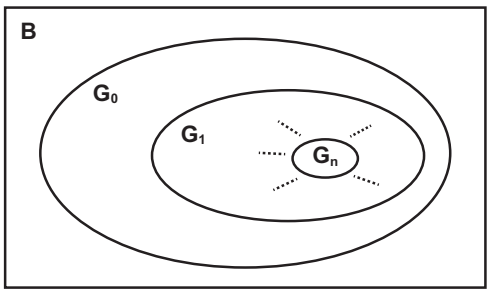

FIG. 1. The progressive reduction of search space by the decomposition algorithm. Here B is the full Pauli operator basis, and $G_0, G_1, \ldots, G_n$ is a decreasing chain of subgroups $(G_{k+1} \subset G_k)$. The algorithm proceeds until one obtains $G_n = \{\mathbb{1}\}$.

where $\alpha,\beta \in \{0,x,y,z\}$. The coefficient $\eta_{\alpha\beta} = i$ if (i) $\alpha \neq \beta$ and (ii) either of $\alpha \in \{0,z\}$ or $\beta \in \{0,z\}$, but not both. For all other cases, $\eta_{\alpha\beta} = 1$.

The product decomposition algorithm [6] proceeds through a systematic reduction of the search space, which is shown schematically in Fig. 1. Let us consider the set

$$\begin{aligned} G_0 = \big\{&\mathbb{1},\sigma_2^x\sigma_3^x,\sigma_2^y\sigma_3^y,\sigma_2^z\sigma_3^z,\sigma_1^x\sigma_4^x,\sigma_1^y\sigma_4^y,\sigma_1^z\sigma_4^z,\\ &\sigma_1^x\sigma_2^x\sigma_3^x\sigma_4^x,\sigma_1^y\sigma_2^y\sigma_3^y\sigma_4^y,\sigma_1^z\sigma_2^z\sigma_3^z\sigma_4^z,\\ &\sigma_1^x\sigma_2^y\sigma_3^y\sigma_4^x,\sigma_1^y\sigma_2^x\sigma_3^x\sigma_4^y,\sigma_1^x\sigma_2^z\sigma_3^z\sigma_4^x,\\ &\sigma_1^z\sigma_2^x\sigma_3^x\sigma_4^z,\sigma_1^y\sigma_2^z\sigma_3^z\sigma_4^y,\sigma_1^z\sigma_2^y\sigma_3^y\sigma_4^z\big\}, \end{aligned} \quad (6)$$

which contains all of the elements from the sum expansion in Eq. (5). This set G_0 forms a group under multiplication of operators. This implies that all of the operators D_k in the product expansion of Eq. (4) belong exclusively to G_0. In cases where G_0 does not form a group by itself, one can add a minimum number of operators from B to G_0 so that G_0 forms a group. Now, consider the set

$$\begin{aligned} G_1 = \big\{&\mathbb{1},\sigma_2^x\sigma_3^x,\sigma_2^y\sigma_3^y,\sigma_2^z\sigma_3^z,\sigma_1^x\sigma_2^x\sigma_3^x\sigma_4^x,\sigma_1^x\sigma_2^y\sigma_3^y\sigma_4^x,\\ &\sigma_1^x\sigma_2^z\sigma_3^z\sigma_4^x,\sigma_1^x\sigma_4^x\big\}, \end{aligned} \quad (7)$$

which is a subgroup of G_0. The set G_1 is selected such that it is a maximal subgroup of G_0. However, this selection need not be unique.

There are a total number of m operators (D_k) in the product decomposition of Eq. (4) and, as said earlier, all of them belong to G_0. Let us suppose that m' of these operators belong to $(G_0 - G_1)$. Then, the next and key step of the algorithm is to find out these m' operators $D_k \in (G_0 - G_1)$ and the corresponding angles θ_k, such that $U_{XY}\prod_{k=1}^{m'}\exp(i\theta_k D_k)$ can be expanded as a sum in B, whose elements belong exclusively to G_1, i.e.,

$$\begin{aligned} U_{XY}\prod_{k=1}^{m'}\exp(i\theta_k D_k) &= U_{XY}^{(m')}\\ &= \sum_r \frac{1}{\tau}\mathrm{Tr}\left(U_{XY}^{(m')}\tilde{D}_r^\dagger\right)\tilde{D}_r, \end{aligned} \quad (8)$$

where $\tilde{D}_r \in G_1$ and $\tau = \mathrm{Tr}(\tilde{D}_r^\dagger\tilde{D}_r)$.

We define the norm of the space spanned by the elements of a set G in a unitary U as

$$N_G(U) = \sum_n |\mathrm{Tr}(U D_n^\dagger)/\mathrm{Tr}(D_n^\dagger D_n)|^2; \quad D_n \in G. \tag{9}$$

The intuitive meaning of norm $N_G(U)$ is to what extent U can be constructed using the elements of G.

For a chosen operator D_k, the angle θ_k is chosen such that the quantity $N_{G_1}(U_{XY}^{(k)}) - N_{G_1}(U_{XY}^{(k-1)})$ is maximized. This leads to

$$\theta_k = \frac{1}{2}\tan^{-1}\left[\frac{W_{k-1}(D_k)}{\Delta_{k-1}}\right], \tag{10}$$

where

$$W_q(D) = \frac{1}{\tau^2}\mathrm{Im}\sum_r \mathrm{Tr}\big(U_{XY}^{(q)}\tilde{D}_r^\dagger\big)\mathrm{Tr}\big(U_{XY}^{(q)}D^\dagger\tilde{D}_r^\dagger\big)^*,$$

$$\Delta_q = N_{G_1}\big(U_{XY}^{(q)}\big) - \frac{1}{2}.$$

The next operator D_{k+1} can be chosen as follows. Calculate the quantity $W_k(D)$ for all of the operators D in $(G_0 - G1)$. Choose the operator D that maximizes $W_k(D)$ as the operator D_{k+1}.

By following the above procedure, we get

$$\begin{aligned} U_{XY}\exp\left(-i\frac{\pi}{4}\sigma_1^y\sigma_2^z\sigma_3^z\sigma_4^y\right) &= \frac{1}{\sqrt{8}}\big[\big(\mathbb{1} + \sigma_2^z\sigma_3^z + \sigma_1^x\sigma_2^x\sigma_3^x\sigma_4^x + \sigma_1^x\sigma_2^y\sigma_3^y\sigma_4^x\big) \\ &\quad + i\big(\sigma_2^x\sigma_3^x + \sigma_2^y\sigma_3^y + \sigma_1^x\sigma_4^x + \sigma_1^x\sigma_2^z\sigma_3^z\sigma_4^x\big)\big], \end{aligned} \tag{11}$$

where all of the operators on the right-hand side belong to G_1. Now consider the set

$$G_2 = \big\{\mathbb{1}, \sigma_2^z\sigma_3^z, \sigma_2^x\sigma_3^x, \sigma_2^y\sigma_3^y\big\}, \tag{12}$$

which is a subgroup of G_1. By repeating the above procedure, we get

$$\begin{aligned} U_{XY}\exp\left(-i\frac{\pi}{4}\sigma_1^y\sigma_2^z\sigma_3^z\sigma_4^y\right)\exp\left(-i\frac{\pi}{4}\sigma_1^x\sigma_2^z\sigma_3^z\sigma_4^x\right) &= \frac{1}{2}\big[\mathbb{1} + \sigma_2^z\sigma_3^z + i\big(\sigma_2^x\sigma_3^x + \sigma_2^y\sigma_3^y\big)\big], \end{aligned} \tag{13}$$

where again all of the operators on the right-hand side belong to G_2.

This process is repeated until we get $G_n = \{\mathbb{1}\}$. Here, by repeating the above procedure two more times with $G_3 = \{\mathbb{1}, \sigma_2^x\sigma_3^x\}$ and $G_4 = \{\mathbb{1}\}$, we get the full product decomposition as

$$\begin{aligned} U_{XY}\exp\left(-i\frac{\pi}{4}\sigma_1^y\sigma_2^z\sigma_3^z\sigma_4^y\right)\exp\left(-i\frac{\pi}{4}\sigma_1^x\sigma_2^z\sigma_3^z\sigma_4^x\right) &\times \exp\left(-i\frac{\pi}{4}\sigma_2^x\sigma_3^x\right)\exp\left(-i\frac{\pi}{4}\sigma_2^y\sigma_3^y\right) = \mathbb{1}, \end{aligned} \tag{14}$$

which can be written as

$$\begin{aligned} U_{XY} &= \exp\left(i\frac{\pi}{4}\sigma_1^y\sigma_2^z\sigma_3^z\sigma_4^y\right)\exp\left(i\frac{\pi}{4}\sigma_1^x\sigma_2^z\sigma_3^z\sigma_4^x\right) \\ &\quad \times \exp\left(i\frac{\pi}{4}\sigma_2^x\sigma_3^x\right)\exp\left(i\frac{\pi}{4}\sigma_2^y\sigma_3^y\right). \end{aligned} \tag{15}$$

B. Five-spin chain

The values of the nearest-neighbor coupling constants for the five-spin XY chain are $J_1 = 2$, $J_2 = \sqrt{6}$, $J_3 = \sqrt{6}$, $J_4 = 2$. The unitary evolution of this five-spin chain for a time $\tau = \pi/2$, i.e., $U_{XY}(\frac{\pi}{2}) = \exp(-i\mathcal{H}\frac{\pi}{2})$, produces the mirror image of any five-spin input state up to a phase difference. For example,

$$\begin{aligned} U_{XY}\left(\frac{\pi}{2}\right)\frac{1}{\sqrt{2}}(|00\rangle + |11\rangle)_{12}|000\rangle_{345} &= |000\rangle_{123}\tfrac{1}{\sqrt{2}}(|00\rangle - |11\rangle)_{45} \end{aligned} \tag{16}$$

and

$$\begin{aligned} U_{XY}\left(\frac{\pi}{2}\right)\frac{1}{\sqrt{2}}(|01\rangle + |10\rangle)_{12}|000\rangle_{345} &= |000\rangle_{123}\tfrac{1}{\sqrt{2}}(|01\rangle + |10\rangle)_{45}. \end{aligned} \tag{17}$$

The above equations show that entangled states can be transferred from one end of the chain to the other up to a phase difference.

By following the procedure similar to that of the four-spin case, the five-spin unitary operator $U_{XY}(\frac{\pi}{2})$ is decomposed into the Pauli operator basis and is given by

$$\begin{aligned} U_{XY}\left(\frac{\pi}{2}\right) &= \exp\left(i\frac{\pi}{2}\sigma_1^x\sigma_2^y\sigma_4^y\sigma_5^x\right)\exp\left(-i\frac{\pi}{4}\sigma_1^x\sigma_2^z\sigma_3^z\sigma_4^z\sigma_5^y\right) \\ &\quad \times \exp\left(-i\frac{\pi}{4}\sigma_1^y\sigma_2^z\sigma_3^z\sigma_4^z\sigma_5^x\right)\exp\left(-i\tfrac{\pi}{4}\sigma_2^x\sigma_3^z\sigma_4^y\right) \\ &\quad \times \exp\left(-i\frac{\pi}{4}\sigma_2^y\sigma_3^z\sigma_4^x\right). \end{aligned} \tag{18}$$

C. *N*-spin chain

The above decomposition can be extended to N-spin XY chains, which are given as follows:

When N is odd,

$$\begin{aligned} U_{XY}\left(\frac{\pi}{2}\right) &= \exp\left(\pm i\frac{\pi}{2}\sigma_1^x\sigma_2^y\sigma_3^x\cdots\mathbb{1}_{\frac{N+1}{2}}\cdots\sigma_{N-2}^x\sigma_{N-1}^y\sigma_N^x\right) \\ &\quad \times \prod_k^{(N-1)/2}\left[\exp\left(\mp i\frac{\pi}{4}\sigma_k^x\sigma_{(N-k+1)}^y\bigotimes_{j=k+1}^{N-k}\sigma_j^z\right)\right. \\ &\quad \left.\times\exp\left(\mp i\frac{\pi}{4}\sigma_k^y\sigma_{(N-k+1)}^x\bigotimes_{j=k+1}^{N-k}\sigma_j^z\right)\right], \end{aligned} \tag{19}$$

where the signs $-$ and $+$ are for chains having $4m+1$ and $4m+3$ (m is an integer) number of spins, respectively, and $\mathbb{1}_{\frac{N+1}{2}}$ is the identity operator for the spin $\frac{N+1}{2}$.

When N is even,

$$\begin{aligned} U_{XY}\left(\frac{\pi}{2}\right) &= \prod_k^{N/2}\left[\exp\left(\pm i\frac{\pi}{4}\sigma_k^x\sigma_{(N-k+1)}^x\bigotimes_{j=k+1}^{N-k}\sigma_j^z\right)\right. \\ &\quad \left.\times\exp\left(\pm i\frac{\pi}{4}\sigma_k^y\sigma_{(N-k+1)}^y\bigotimes_{j=k+1}^{N-k}\sigma_j^z\right)\right], \end{aligned} \tag{20}$$

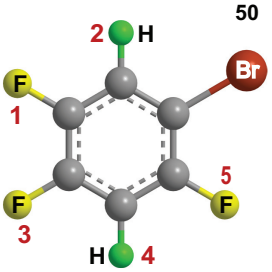

1	2	3	4	5	
-6743	1532	-26	55	116	1
	50	106	-7.6	54	2
		-3680	1270	277	3
			29	1556	4
				6029	5

FIG. 2. (Color online) Chemical structure of the molecule and Hamiltonian parameters. In the table, diagonal elements correspond to the Zeeman shifts (ν_i) of the nuclear spins (in Hz) in the doubly rotating frame and the off-diagonal elements correspond to the coupling constants ($J_{ij} + 2D_{ij}$) between them (in Hz).

where the signs + and − are for chains having $4m$ and $4m + 2$ (m is an integer) number of spins, respectively.

The unitary operators in the right-hand side of Eqs. (15) and (18) can be further decomposed into single-qubit rotations and two-qubit gates [30]. Conventional pulse sequences can be constructed by using these decompositions to realize the full unitary evolution. However, in the experimental implementation, we realized each of the decomposed operators with a single GRAPE pulse. We now describe the experimental simulation of the above four- and five-spin chains using NMR techniques.

III. EXPERIMENTAL IMPLEMENTATION

We choose 1-bromo-2,4,5-trifluorobenzene partially oriented in a liquid-crystal medium, N-(4-methoxybenzaldehyde)-4-butylaniline (MBBA), as our spin system for the experimental implementation [36]. The three ^{19}F and two ^{1}H nuclei form a five-spin system. These spins are labeled as 1–5, as shown in Fig. 2. The effective transverse relaxation times (T_2^*) of the transitions of spins 1, 3, and 5 (fluorine nuclei) are in the range 40–60, 40–60, and 60–100 ms, respectively, and that of the transitions of spins 2 and 4 (proton nuclei) are in the range 140–150 and 110–150 ms, respectively. These are calculated from the inverse of the observed linewidths, which are mainly governed by the director fluctuation in a liquid crystal and are an order of magnitude larger than the linewidths in isotropic solutions. All of the experiments have been carried out at an ambient temperature of 300 K on a Bruker AVIII 500 MHz NMR spectrometer using a QXI probe.

Due to the partial orientational order of the liquid-crystal medium, the direct dipolar couplings among the spins do not get fully averaged out, but get scaled down by the order parameter. Depending on the order parameter of the liquid-crystal medium, the residual dipolar couplings between the spins are an order of magnitude stronger than the indirect scalar couplings. The Zeeman shift values of the nuclear spins and the coupling constants between them are given in Fig. 2. The Hamiltonian for the dipolar interaction between the heteronuclear spins is of the form $\mathcal{H}_D = \frac{\pi}{2}\sum_{i,j(i<j)} D_{ij}\, 2\sigma_i^z\sigma_j^z$, where D_{ij} is the scaled dipolar coupling constant, and the same between the homonuclear spins is of the form $\mathcal{H}_D = \frac{\pi}{2}\sum_{i,j(i<j)} D_{ij}(3\sigma_i^z\sigma_j^z - \sigma_i\cdot\sigma_j)$. Since, the difference between Zeeman shifts of any pair of spins is much larger than the respective dipolar coupling between them, the Hamiltonian for the homonuclear dipolar interaction can be approximated to $\mathcal{H}_D = \frac{\pi}{2}\sum_{i,j(i<j)} D_{ij} 2\sigma_i^z\sigma_j^z$. Hence, the full Hamiltonian of the spin system in the doubly rotating frame can be written as

$$\mathcal{H}_{\rm NMR} = -\pi\sum_i \nu_i\sigma_i^z + \frac{\pi}{2}\sum_{i,j(i<j)}(J_{ij} + 2D_{ij})\sigma_i^z\sigma_j^z, \quad (21)$$

where ν_i is the Zeeman shift of the spin i and J_{ij} is the scalar coupling constant between the spins i and j. The magnitude of the coupling constants ($J_{ij} + 2D_{ij}$) was obtained by fitting equilibrium spectra of the spin system and the sign of them was determined by performing heteronuclear z-COSY experiments [37–39].

The equilibrium deviation density matrix of the spin system under high-temperature and high-field approximation can be represented by [40]

$$\rho_{\rm eq}^{\Delta} = \gamma_{\rm F}\left(\sigma_z^1 + \sigma_z^3 + \sigma_z^5\right) + \gamma_{\rm H}\left(\sigma_z^2 + \sigma_z^4\right), \quad (22)$$

where $\gamma_{\rm H}$ and $\gamma_{\rm F} = 0.94\gamma_{\rm H}$ are gyromagnetic ratios of the nuclei ^{19}F and ^{1}H, respectively.

The five-spin NMR system has been used to demonstrate the mirror-inversion operation in the following XY chains: (i) a five-spin chain, prepared in mixed or subsystem pseudopure initial states and (ii) a four-spin chain prepared in pseudopure initial states. We used the GRAPE [2] technique to realize the product decompositions of the mirror-inversion propagators of four- and five-spin XY chains, which are given in Eqs. (15) and (18). Each of the unitary operators in the right-hand side of these equations has been realized using a single GRAPE pulse. The total length of these pulses for realizing the mirror-inversion propagator of a four-spin chain is 34 ms and the same for a five-spin chain is 40 ms. All of the GRAPE pulses were optimized such that they are robust against rf field inhomogeneity and the average Hilbert-Schmidt fidelity [41] of all of these pulses is greater than 0.99.

A. Five-spin initial states

Coherence transfer. The mirror-inversion operation can be used to transfer single quantum coherence of a spin to its mirror image (in-phase to antiphase). Here, we perform two different experiments with respective initial states (i) σ_1^x and (ii) σ_2^x. These initial states were prepared from the equilibrium state as follows. We first apply a spin-selective $(\pi/2)^x$ pulse on spin 1 (2) and then a $(\pi/2)^{-x}$ pulse on all of the spins followed by a gradient pulse in the z direction. This saturates the magnetization of all of the spins except spin 1 (2). We now apply a spin-selective $(\pi/2)^y$ pulse on spin 1 (2), which produces the desired initial state σ_1^x (σ_2^x). All the spin-selective and global pulses used here and henceforth were realized using the GRAPE technique [2]. The lengths of the spin-selective pulses on fluorine spins (1, 3, and 5) are in the range 500–600 μs, and those on the proton spins 2 and 4 are 2.5 and 3 ms, respectively. The length of the $\pi/2$ pulse on all of the spins is 500 μs. The resultant spectra, which confirm the creation of

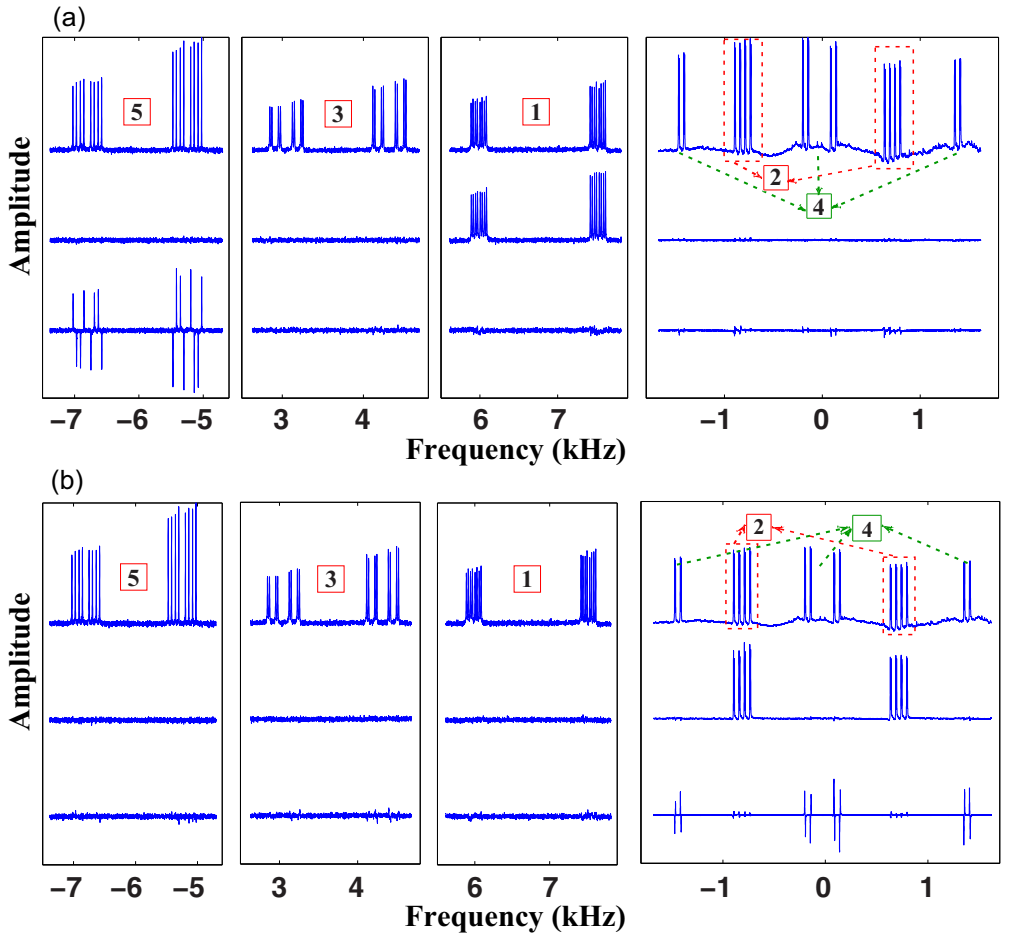

FIG. 3. (Color online) Experimental results for single quantum coherence transfer. (a) Transfer from spin 1 to its mirror image, spin 5, and (b) transfer from spin 2 to its mirror image, spin 4. In both (a) and (b) the top row corresponds to the equilibrium spectra, the middle row represents spectra corresponding to the initial state, and the bottom row is that of the final state.

the initial states, are shown in the middle trace of Figs. 3(a) and 3(b). The application of the unitary operator in Eq. (18) on the initial states σ_1^x and σ_2^x produces the states $\sigma_1^z\sigma_2^z\sigma_3^z\sigma_4^z\sigma_5^x$ and $\sigma_1^z\sigma_2^z\sigma_3^z\sigma_4^x\sigma_5^z$, respectively. This clearly demonstrates that the coherence of spin 1 (2) is transferred to its mirror image 5 (4). The transferred coherence is antiphase with respect to all other spins; this is due to the relative phase difference between different many-particle subspaces. The experimental spectra corresponding to the final states are shown in the bottom trace of Figs. 3(a) and 3(b). The clear antiphase signals for the spins 5 and 4 and the absence of signals for all the other spins indicate the efficient implementation of the mirror-inversion operation.

Entanglement transfer. As discussed in the previous section, mirror-inversion operation can also be used to transfer entangled states from one end of the chain to the other. We initially prepare maximally entangled states of spins 1 and 2. The unitary evolution of the spin chain drives these entangled states to their mirror images, i.e., spins 4 and 5. We choose the initial states as $\frac{1}{16}(|00\rangle + |11\rangle)(\langle 00| + \langle 11|)_{12} \otimes \mathbb{1}_3 \otimes \mathbb{1}_4 \otimes \mathbb{1}_5$ and $\frac{1}{16}(|01\rangle + |10\rangle)(\langle 01| + \langle 10|)_{12} \otimes \mathbb{1}_3 \otimes \mathbb{1}_4 \otimes \mathbb{1}_5$, where spins 1 and 2 are in the maximally entangled state and all other spins are in the maximally mixed state. These initial states were prepared from the equilibrium as described below. We first prepare the spins 1 and 2 in the $|00\rangle$ pseudopure state using the spatial-averaging technique [42] and all the other spins in the maximally mixed state by dephasing their magnetization. The pulse sequence, used to create the state $\frac{1}{8}|00\rangle\langle 00|_{12} \otimes \mathbb{1}_3 \otimes \mathbb{1}_4 \otimes \mathbb{1}_5$ from equilibrium, is given by

$$\left[\frac{\pi}{2}\right]_x^{1,2} - \left[\frac{\pi}{2}\right]_{-x}^{\mathrm{All}} - \left[G\right]_z - \left[0.32\pi\right]_x^1 - \left[G\right]_z - \left[\frac{\pi}{4}\right]_x^2 - \left[\frac{1}{2(J+2D)_{12}}\right] - \left[\frac{\pi}{4}\right]_{-y}^2 - \left[G\right]_z, \quad (23)$$

where $[\theta]_\alpha^i$ denotes a θ degree pulse on spin i about the axis α, $[G]_z$ denotes a gradient pulse along the z direction, and $[\frac{1}{2(J+2D)_{ij}}]$ represents coupling evolution of spins i,j for a period $\frac{1}{2(J+2D)_{ij}}$. Here, the two $\pi/4$ pulses on spin 2 and the coupling evolution in between were combined and realized using a single GRAPE pulse. The length of this pulse is 2.4 ms. The state $\frac{1}{8}|10\rangle\langle 10|_{12} \otimes \mathbb{1}_3 \otimes \mathbb{1}_4 \otimes \mathbb{1}_5$ can be prepared from the state $\frac{1}{8}|00\rangle\langle 00|_{12} \otimes \mathbb{1}_3 \otimes \mathbb{1}_4 \otimes \mathbb{1}_5$ by applying a π pulse on spin 1. The desired initial states $\frac{1}{16}(|00\rangle + |11\rangle)(\langle 00| + \langle 11|)_{12} \otimes \mathbb{1}_3 \otimes \mathbb{1}_4 \otimes \mathbb{1}_5$ and $\frac{1}{16}(|01\rangle + |10\rangle)(\langle 01| + \langle 10|)_{12} \otimes \mathbb{1}_3 \otimes \mathbb{1}_4 \otimes \mathbb{1}_5$ were prepared by applying the unitary operator

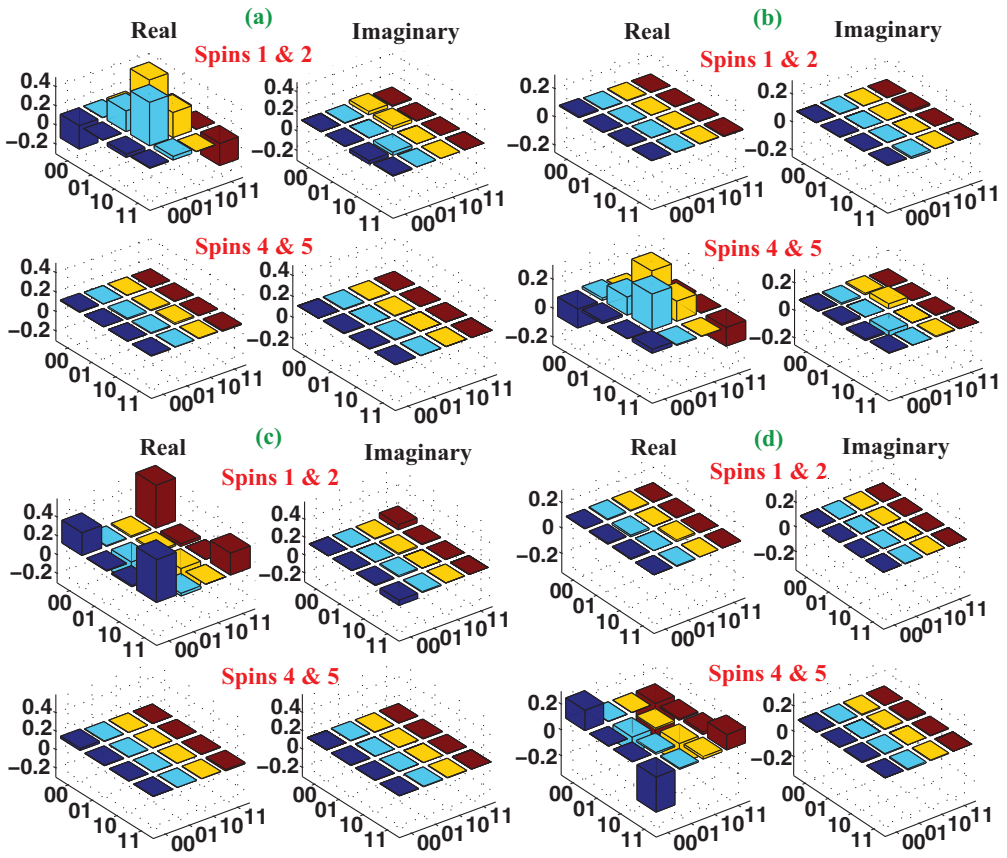

FIG. 4. (Color online) Experimental results for entanglement transfer. Reconstructed deviation density matrices (traceless) of spins 1 and 2, and spins 4 and 5, for (a) the initial state $\frac{1}{2}(|01\rangle + |10\rangle)(\langle 01| + \langle 10|)_{12} \otimes \mathbb{1}_3 \otimes \mathbb{1}_4 \otimes \mathbb{1}_5$, (b) the final state $\mathbb{1}_1 \otimes \mathbb{1}_2 \otimes \mathbb{1}_3 \otimes \frac{1}{2}(|01\rangle + |10\rangle)(\langle 01| + \langle 10|)_{45}$, (c) the initial state $\frac{1}{2}(|00\rangle + |11\rangle)(\langle 00| + \langle 11|)_{12} \otimes \mathbb{1}_3 \otimes \mathbb{1}_4 \otimes \mathbb{1}_5$, and (d) the final state $\mathbb{1}_1 \otimes \mathbb{1}_2 \otimes \mathbb{1}_3 \otimes \frac{1}{2}(|00\rangle - |11\rangle)(\langle 00| - \langle 11|)_{45}$.

$\exp(-i\frac{\pi}{4}\sigma_1^x\sigma_2^y)$ to the states $|00\rangle\langle 00|_{12} \otimes \mathbb{1}_3 \otimes \mathbb{1}_4 \otimes \mathbb{1}_5$ and $|10\rangle\langle 10|_{12} \otimes \mathbb{1}_3 \otimes \mathbb{1}_4 \otimes \mathbb{1}_5$, respectively. This unitary operator was also realized using a GRAPE pulse and its length is 2.4 ms.

Applying the mirror-inversion propagator of Eq. (18) to the above initial states leads to

$$\tfrac{1}{16}(|00\rangle + |11\rangle)(\langle 00| + \langle 11|)_{12} \otimes \mathbb{1}_3 \otimes \mathbb{1}_4 \otimes \mathbb{1}_5 \longrightarrow \tfrac{1}{16}\mathbb{1}_1 \otimes \mathbb{1}_2 \otimes \mathbb{1}_3 \otimes (|00\rangle - |11\rangle)(\langle 00| - \langle 11|)_{45}, \quad (24)$$

$$\tfrac{1}{16}(|01\rangle + |10\rangle)(\langle 01| + \langle 10|)_{12} \otimes \mathbb{1}_3 \otimes \mathbb{1}_4 \otimes \mathbb{1}_5 \longrightarrow \tfrac{1}{16}\mathbb{1}_1 \otimes \mathbb{1}_2 \otimes \mathbb{1}_3 \otimes (|01\rangle + |10\rangle)(\langle 01| + \langle 10|)_{45}, \quad (25)$$

where now spins 1–3 are in the maximally mixed state, and spins 4 and 5 are in the maximally entangled state.

To confirm the creation and transfer of entangled states, we have performed quantum state tomography of two-spin subsystems containing spins 1, 2 and 4, 5 for both initial and final states. The tomography results for both the initial and final states are shown in Fig. 4.

To quantitatively evaluate the experimental results, we compare the experimental deviation (traceless) density matrices with the theoretically expected ones by using the following measures. (i) *Correlation*. The correlation (c) between the experimental deviation density matrices and the theoretically expected ones is defined as [1,43]

$$c = \frac{\mathrm{tr}(\rho_{\mathrm{th}}^{\Delta}\rho_{\mathrm{expt}}^{\Delta})}{\sqrt{\mathrm{tr}[(\rho_{\mathrm{th}}^{\Delta})^2]\mathrm{tr}[(\rho_{\mathrm{expt}}^{\Delta})^2]}}. \quad (26)$$

It quantifies how similar in direction the two deviation density matrices are, analogous to the dot product between two vectors. To also account for the net loss of magnetization due to the nonunitary evolution, we use the measure (ii) *attenuated correlation* (ac) [44], defined as

$$ac = \frac{\mathrm{tr}(\rho_{\mathrm{th}}^{\Delta}\rho_{\mathrm{expt}}^{\Delta})}{\mathrm{tr}[(\rho_{\mathrm{th}}^{\Delta})^2]}. \quad (27)$$

The correlations and attenuated correlations of all of the initial and final states are given in Table I. The high correlations between the experimental and theoretically expected deviation density matrices of both the initial and final states indicate the efficient creation and transfer of entangled states. The low values of attenuated correlations of the final states can be attributed to the nonunitary evolution caused by decoherence during the experiment, as the total time of the experiment (≈52 ms including the preparation of initial state) is comparable to the T_2^* of the fluorine spins.

TABLE I. Correlation and attenuated correlation of all the initial and final entangled states.

	Correlation	Attenuated correlation		Correlation	Attenuated correlation
Initial State I			Initial State II		
$\frac{1}{16}(\|00\rangle + \|11\rangle)(\langle 00\| + \langle 11\|)_{12} \otimes \mathbb{1}_3 \otimes \mathbb{1}_4 \otimes \mathbb{1}_5$			$\frac{1}{16}(\|01\rangle + \|10\rangle)(\langle 01\| + \langle 10\|)_{12} \otimes \mathbb{1}_3 \otimes \mathbb{1}_4 \otimes \mathbb{1}_5$		
Spins 1& 2	0.992	0.926	Spins 1 & 2	0.991	0.921
Spins 4 & 5	0.998		Spins 4 & 5	0.998	
Final State I			Final State II		
$\frac{1}{16}\mathbb{1}_1 \otimes \mathbb{1}_2 \otimes \mathbb{1}_3 \otimes (\|00\rangle - \|11\rangle)(\langle 00\| - \langle 11\|)_{45}$			$\frac{1}{16}\mathbb{1}_1 \otimes \mathbb{1}_2 \otimes \mathbb{1}_3 \otimes (\|01\rangle + \|10\rangle)(\langle 01\| + \langle 10\|)_{45}$		
Spins 1 & 2	0.998		Spins 1 & 2	0.998	
Spins 4 & 5	0.993	0.545	Spins 4 & 5	0.986	0.504

B. Four-spin pseudopure initial states

The spatially averaged logical labeling technique (SALLT) [45] was used to prepare four-spin pseudopure states in a five-spin system as described below. Here, the Hilbert space of the five-spin system is divided into two four-spin subspaces based on the $|0\rangle$ and $|1\rangle$ states of spin 5, which do not take part in the mirror-inversion operation. Starting from equilibrium, we dephased the magnetization of all spins except spin 5, by using the procedure described earlier in Sec. III A. Then, the state of the spin system can be described by the density operator σ_5^z. The desired four-spin pseudopure states (in each of the two subspaces corresponding to the $|0\rangle$ and $|1\rangle$ states of spin 5) were prepared from the state σ_5^z by flipping (π rotation) the corresponding transition of spin 5. For example, the $|0000\rangle$ pseudopure state (labeled by the states of spins 1 to 4) was prepared by inverting the $|00000\rangle \leftrightarrow |00001\rangle$ transition of spin 5. A representative diagram for the deviation populations of the $|0000\rangle$ pseudopure state is given in Fig. 5. Note that the deviation populations in both of the subspaces (of spin 5) are the same but are opposite in sign.

By using the above method, we prepared the $|1000\rangle\langle 1000|$, $|1010\rangle\langle 1010|$, and $|1110\rangle\langle 1110|$ initial pseudopure states. All of the transition-selective π pulses were implemented by Gaussian-shaped pulses of duration 40 ms. The above initial states were transformed into their mirror images $|0001\rangle\langle 0001|$, $|0101\rangle\langle 0101|$, and $|0111\rangle\langle 0111|$, respectively, by the unitary operator in Eq. (15).

Diagonal tomography of all of the initial and final states was performed by applying a gradient pulse followed by a $\pi/2$ pulse on each spin separately, and fitting the resultant single quantum spectra. The results along with the theoretically expected ones are shown in Fig. 6. The bar plots shown in the figure represent the diagonal deviation density matrices (traceless) of spins 1 to 4. These are obtained by taking the average over the deviation populations of the two subspaces of spin 5, where the sign of deviation populations of one of the two subspaces is reversed, and then subtracting the trace. The correlations of the experimental diagonal deviation density matrices with respect to the theoretically expected ones are calculated and the results are as follows. The diagonal correlations of all the initial states are better than 0.994 and those of all the final states are better than 0.989. The high correlation of the final states confirms the successful implementation of the mirror-inversion operation on pseudopure initial states.

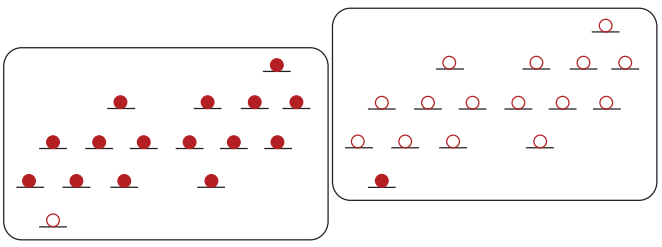

FIG. 5. (Color online) A representative energy-level diagram and deviation populations for the $|0000\rangle$ pseudopure state. The filled and open circles represent the positive and negative deviation populations (with respect to the background population), respectively.

IV. DISCUSSION

Here, we compare the simulation of mirror-inversion propagators described in this work with the mirror-inversion operation by a set of two-qubit SWAP gates in the case of spin chains having only nearest-neighbor interactions. To realize the full mirror-inversion operation in a four-spin chain, six two-qubit SWAP gates are needed, and for the same in a five-spin chain, ten two-qubit SWAP gates are needed. Each two-qubit SWAP gate is implemented by a sequence of XX [$\exp(-i\pi/4\sigma_x^i\sigma_x^j)$], YY [$\exp(-i\pi/4\sigma_y^i\sigma_y^j)$], and ZZ [$\exp(-i\pi/4\sigma_z^i\sigma_z^j)$] gates [46]. So, a total of 18 two-qubit gates are required in the case of a four-spin chain, and 30 two-qubit gates are required in the case of a five-spin chain.

Now, let us see the number of two-qubit gates required to realize the product decompositions of the mirror-inversion propagators described in this work. The propagator of the four-spin chain is decomposed into two four-spin generators and two two-spin generators. Each four-spin generator can be implemented by five two-qubit (nearest-neighbor) gates (such as ZZ, XX) [30]. So, a total of 12 two-qubit gates are needed to realize the four-spin mirror-inversion propagator. By a similar line of argument, a total of 27 ($7 + 7 + 7 + 3 + 3$) two-qubit (nearest-neighbor) gates are needed to realize the five-spin propagator. Note also that the mirror-inversion operation realized in this paper is exact for the input states from each excitation subspace, but may not be exact for the input states, which have superpositions from different excitation subspaces. Overall, we point out that the number of two-qubit gates required for our simulation, and that required

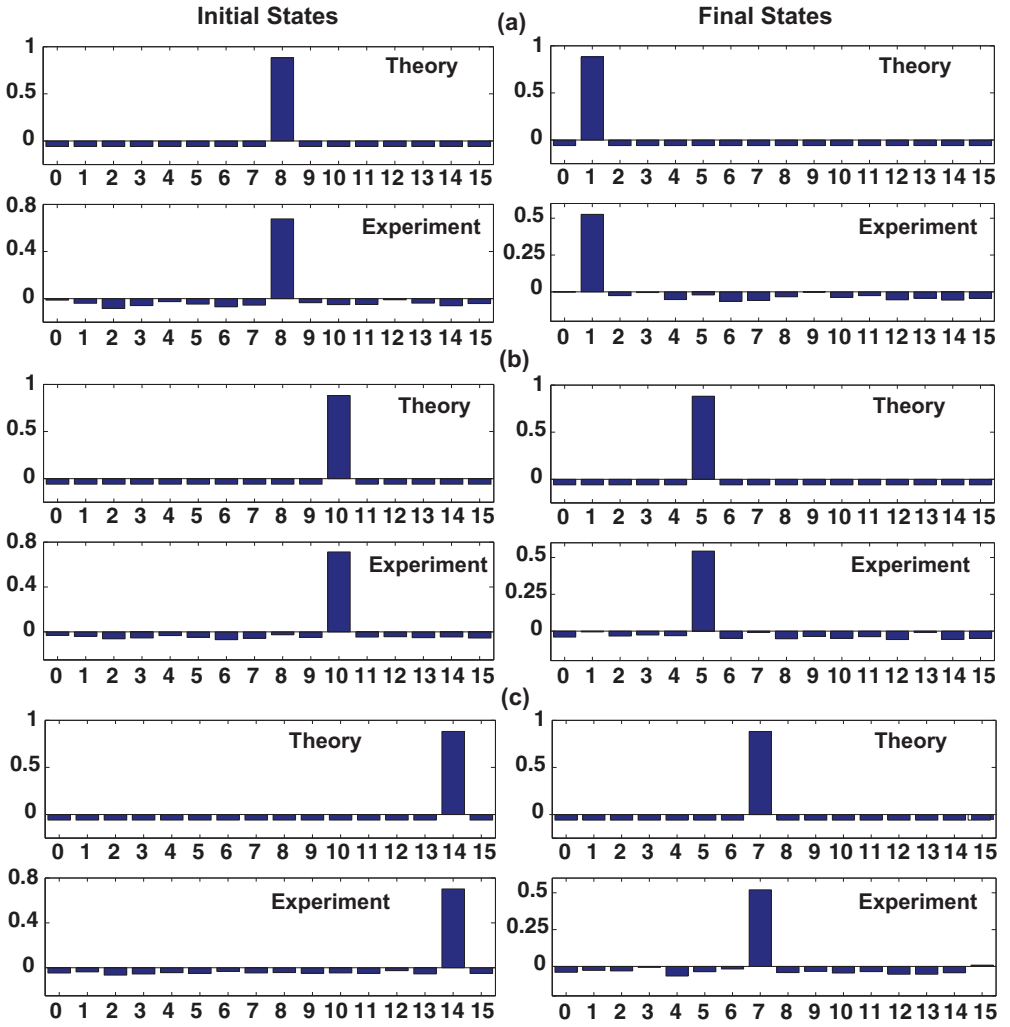

FIG. 6. (Color online) The theoretically expected and the experimentally reconstructed diagonal deviation density matrices (traceless; top and bottom rows in each case, respectively) for the initial (left column) and final (mirror-inverted; right column) pseudopure states, (a) $|1000\rangle\langle 1000| \rightarrow |0001\rangle\langle 0001|$, (b) $|1010\rangle\langle 1010| \rightarrow |0101\rangle\langle 0101|$, and (c) $|1110\rangle\langle 1110| \rightarrow |0111\rangle\langle 0111|$. The x axes represent the standard computational basis in decimal form and the y axes represent the amplitude of the corresponding elements.

for a mirror-inversion operation through a set of SWAP gates, in a nearest-neighbor setting, are of the same order.

V. CONCLUSION

It is demonstrated that the combination of two different numerical algorithms, i.e., one is a unitary operator decomposition algorithm and the other is a pulse optimization algorithm, can yield high experimental fidelities in precise implementations of arbitrary unitary operators. Combining these two algorithms also saves a lot of time during numerical optimization. To illustrate the method, we simulated the mirror-inversion propagator of an engineered *XY* spin chain. This propagator has been chosen because of its simple product decomposition into the Pauli operator basis, which scales only linearly with the number of qubits. The simulation has also been used to demonstrate the transfer of entangled states from one end of the chain to the other end. The presented method is expected to work well for all of the unitary operators, which have polynomial product decompositions. This method can also be combined with the subsystems approach given in Refs. [31,32] to extend the simulations to larger spin systems.

[1] E. M. Fortunato, M. A. Pravia, N. Boulant, G. Teklemariam, T. F. Havel, and D. G. Cory, J. Chem. Phys. **116**, 7599 (2002).
[2] N. Khaneja, T. Reiss, C. Kehlet, T. Schulte-Herbruggen, and S. J. Glaser, J. Magn. Reson. **172**, 296 (2005).
[3] R. R. Tucci, arXiv:quant-ph/9902062.
[4] N. Khaneja and S. J. Glaser, Chem. Phys. **267**, 11 (2001).
[5] J. J. Vartiainen, M. Möttönen, and M. M. Salomaa, Phys. Rev. Lett. **92**, 177902 (2004).
[6] A. Ajoy, R. K. Rao, A. Kumar, and P. Rungta, Phys. Rev. A **85**, 030303 (2012).

[7] C. Albanese, M. Christandl, N. Datta, and A. Ekert, Phys. Rev. Lett. **93**, 230502 (2004).
[8] S. Bose, Phys. Rev. Lett. **91**, 207901 (2003).
[9] M. Christandl, N. Datta, A. Ekert, and A. J. Landahl, Phys. Rev. Lett. **92**, 187902 (2004).
[10] M. Christandl, N. Datta, T. C. Dorlas, A. Ekert, A. Kay, and A. J. Landahl, Phys. Rev. A **71**, 032312 (2005).
[11] G. M. Nikolopoulos, D. Petrosyan, and P. Lambropoulos, J. Phys. Condens. Matter **16**, 4991 (2004).
[12] G. M. Nikolopoulos, D. Petrosyan, and P. Lambropoulos, Europhys. Lett. **65**, 297 (2004).
[13] S. Bose, Contemp. Phys. **48**, 13 (2007).
[14] A. Kay, Int. J. Quantum Inf. **08**, 641 (2010).
[15] P. Karbach and J. Stolze, Phys. Rev. A **72**, 030301 (2005).
[16] J. Fitzsimons and J. Twamley, Phys. Rev. Lett. **97**, 090502 (2006).
[17] D. Burgarth, V. Giovannetti, and S. Bose, Phys. Rev. A **75**, 062327 (2007).
[18] P. Cappellaro, C. Ramanathan, and D. G. Cory, Phys. Rev. Lett. **99**, 250506 (2007).
[19] C. Di Franco, M. Paternostro, and M. S. Kim, Phys. Rev. Lett. **101**, 230502 (2008).
[20] L. Banchi, T. J. G. Apollaro, A. Cuccoli, R. Vaia, and P. Verrucchi, Phys. Rev. A **82**, 052321 (2010).
[21] L. Banchi, T. J. G. Apollaro, A. Cuccoli, R. Vaia, and P. Verrucchi, New J. Phys. **13**, 123006 (2011).
[22] A. Ajoy and P. Cappellaro, Phys. Rev. A **85**, 042305 (2012).
[23] J. Zhang, G. L. Long, W. Zhang, Z. Deng, W. Liu, and Z. Lu, Phys. Rev. A **72**, 012331 (2005).
[24] J. Zhang, N. Rajendran, X. Peng, and D. Suter, Phys. Rev. A **76**, 012317 (2007).
[25] J. Fitzsimons, L. Xiao, S. C. Benjamin, and J. A. Jones, Phys. Rev. Lett. **99**, 030501 (2007).
[26] P. Cappellaro, C. Ramanathan, and D. G. Cory, Phys. Rev. A **76**, 032317 (2007).
[27] J. Zhang, M. Ditty, D. Burgarth, C. A. Ryan, C. M. Chandrashekar, M. Laforest, O. Moussa, J. Baugh, and R. Laflamme, Phys. Rev. A **80**, 012316 (2009).
[28] G. A. Álvarez, M. Mishkovsky, E. P. Danieli, P. R. Levstein, H. M. Pastawski, and L. Frydman, Phys. Rev. A **81**, 060302 (2010).
[29] K. R. K. Rao and A. Kumar, Int. J. Quantum Info. **10**, 1250039 (2012).
[30] C. H. Tseng, S. Somaroo, Y. Sharf, E. Knill, R. Laflamme, T. F. Havel, and D. G. Cory, Phys. Rev. A **61**, 012302 (1999).
[31] C. Negrevergne, T. S. Mahesh, C. A. Ryan, M. Ditty, F. Cyr-Racine, W. Power, N. Boulant, T. Havel, D. G. Cory, and R. Laflamme, Phys. Rev. Lett. **96**, 170501 (2006).
[32] C. A. Ryan, C. Negrevergne, M. Laforest, E. Knill, and R. Laflamme, Phys. Rev. A **78**, 012328 (2008).
[33] P. Diehl and C. L. Khetrapal, *NMR Basic Principles and Progress*, edited by P. Diehl, E. Fluck, and R. Kosfeld (Springer-Verlag, Berlin, 1969), Vol. 1, pp. 1–95.
[34] C. S. Yannoni, M. H. Sherwood, D. C. Miller, I. L. Chuang, L. M. K. Vandersypen, and M. G. Kubinec, Appl. Phys. Lett. **75**, 3563 (1999).
[35] T. S. Mahesh and D. Suter, Phys. Rev. A **74**, 062312 (2006).
[36] A. Shukla, K. R. K. Rao, and T. S. Mahesh, Phys. Rev. A **87**, 062317 (2013).
[37] H. Oschkinat, A. Pastore, P. Pfndler, and G. Bodenhausen, J. Magn. Reson. **69**, 559 (1986).
[38] R. R. Grace and A. Kumar, J. Magn. Reson. **99**, 81 (1992).
[39] R. Das, R. Bhattacharyya, and A. Kumar, J. Magn. Reson. **170**, 310 (2004).
[40] R. R. Ernst, G. Bodenhausen, and A. Wokaun, *Principles of Nuclear Magnetic Resonance in One and Two Dimensions* (Oxford University Press, Oxford, 1990).
[41] M. A. Nielsen, Phys. Lett. A **303**, 249 (2002).
[42] D. G. Cory, M. D. Price, and T. F. Havel, Physica D **120**, 82 (1998).
[43] M. A. Pravia, N. Boulant, J. Emerson, A. Farid, E. M. Fortunato, T. F. Havel, R. Martinez, and D. G. Cory, J. Chem. Phys. **119**, 9993 (2003).
[44] G. Teklemariam, E. M. Fortunato, M. A. Pravia, T. F. Havel, and D. G. Cory, Phys. Rev. Lett. **86**, 5845 (2001).
[45] T. S. Mahesh and A. Kumar, Phys. Rev. A **64**, 012307 (2001).
[46] Z. L. Madi, R. Bruschweiler, and R. R. Ernst, J. Chem. Phys. **109**, 10603 (1998).